HHS Public Access

Author manuscript

Nat Struct Mol Biol. Author manuscript; available in PMC 2019 April 05.

Published in final edited form as:

Nat Struct Mol Biol. 2018 October ; 25(10): 911–917. doi:10.1038/s41594-018-0130-9.

A molecular mechanism for calcium/synaptotagmin-triggered exocytosis

Volker Kiessling[1,2,*], **Alex J.B. Kreutzberger**[1,2], **Binyong Liang**[1,2], **Sarah B. Nyenhuis**[3], **Patrick Seelheim**[1,2], **J. David Castle**[4], **David S. Cafiso**[3], and **Lukas K. Tamm**[1,2]

[1]Center for Membrane and Cell Physiology University of Virginia, Charlottesville, Virginia, USA.

[2]Department of Molecular Physiology and Biological Physics University of Virginia, Charlottesville, Virginia, USA.

[3]Department of Chemistry University of Virginia, Charlottesville, Virginia, USA.

[4]Department of Cell Biology University of Virginia, Charlottesville, Virginia, USA.

Abstract

The regulated exocytotic release of neurotransmitter and hormones is accomplished by a complex protein machinery consisting in its core of SNARE proteins and the calcium sensor synaptotagmin-1. We propose a mechanism where the lipid membrane is intimately involved in coupling calcium sensing to release. We demonstrate that fusion of dense core vesicles, derived from rat PC12 cells is strongly linked to the angle between the cytoplasmic domain of the SNARE complex and the plane of the target membrane. We propose that, as this tilt angle increases, force is exerted on the SNARE transmembrane domains to drive the merger of the two bilayers. The tilt angle dramatically increases upon calcium-mediated binding of synaptotagmin to membranes, strongly depends on the surface electrostatics of the membrane, and is strictly coupled to lipid order of the target membrane.

Introduction

Neurons and other secretory cells release neurotransmitters or hormones into the extracellular space by exocytosis in response to a rise of intracellular Ca^{2+} levels near the release site. Ca^{2+}-regulated exocytosis is accomplished by a set of essential proteins that catalyze fusion of the secretory vesicle with the plasma membrane. The regulatory precision of this process is particularly rigorous in synaptic transmission where synaptic vesicles release their neurotransmitter content within tens of microseconds after the plasma membrane has been depolarized and Ca^{2+} channels have opened to raise the intracellular Ca^{2+} concentration [1,2]. Intense research over the last two decades has identified not only the

*Correspondence to: vgk3c@virginia.edu.

Author contributions :V.K. performed and analyzed all sdFLIC experiments. A.J.B.K. performed and analyzed all DCV fusion experiments. B.L. and S.N. prepared protein samples. P.S. prepared shRNA for SytKD DCVs. V.K. designed the work. V. K., D.S.C., J.D.C., and L.K.T. wrote the paper.

Competing financial interests: The authors declare no competing financial interests.

proteins that are essential, but also some of the necessary steps in regulated exocytosis. The final steps include a relatively loose tethering of secretory vesicles at the active zones of presynaptic membranes, docking to immobilize those vesicles, and priming that renders the fusion machinery highly sensitive to Ca^{2+} [3–5]. Essential membrane proteins for this process are the SNARE proteins syntaxin-1a (Syx1a) and SNAP-25 in the plasma membrane and synaptobrevin-2/VAMP-2 (Syb2) in the synaptic vesicle membrane, as well as different isoforms of synaptotagmin (Syt) in the vesicle membrane [6]. Syt1 is the isoform that is most relevant for fast, evoked neurotransmitter release in neurons.

During fusion, the cytosolic domains of SNARE proteins, specifically their SNARE motifs, assemble into a highly stable four-helix bundle termed the SNARE complex. SNARE proteins alone are sufficient to catalyze membrane fusion when reconstituted in purified form into proteoliposomes, albeit in a Ca^{2+}-independent fashion [7]. The cytosolic part of Syt consists of two C2 domains that have been identified as the Ca^{2+} sensors for Ca^{2+}-triggered exocytosis [8]. In vitro fusion experiments with reconstituted proteoliposomes that consist only of SNAREs, Syt1 and negatively charged lipids show a Ca^{2+}-dependent increase of fusion events [9–14]. However, compared to regulated exocytosis, these systems all exhibit a relatively high base-level of fusion in the absence of Ca^{2+}. Therefore, it is clear that other proteins are essential to achieve the precise regulation that is observed in synaptic neurotransmitter release. These include SM (Sec1/Munc18-like) proteins, complexins, and Munc13-like proteins [3,5,15,16].

While the importance of several of these regulatory proteins has been identified, their precise function during docking, priming, and fusion-triggering is still debated. Of particular interest is the molecular architecture of the primed state. The physiological stoichiometries of these fusion-ready assemblies are frequently not known and whether full-length or only fragments of these multi-domain proteins are used often determines the outcomes of in-vitro experiments. Finally, despite its effects on synaptic function and brain health [17], the role of the surrounding membrane and the complexity of its lipid composition have been frequently ignored. Reconstitution experiments show that significant Ca^{2+}-dependent increases in fusion efficiency can be achieved when Munc18 and Munc13's MUN domain [18] or complexin [14] are included in SNARE/Syt fusion assays. Our lab recently developed an assay that resolves the docking and fusion of single purified dense-core vesicles (DCVs) from PC12 cells with supported membranes that contain acceptor t-SNAREs (i.e., full-length Syx1a and SNAP-25A) that had been activated by Munc18–1 and restricted for fusion in the absence of Ca^{2+} by complexin (Fig. 1b) [19]. Injection of moderate amounts (tens of μM) of Ca^{2+} triggered fusion from near-zero to ~70% probability under known physiological protein and lipid conditions that closely approximate triggering of neuronal exocytosis (Fig. 1e black trace, adapted from Ref.[19]). In the absence of Munc18 and complexin, SNARE/Syt fusion can still be triggered by the same level of Ca^{2+}, but unrestricted (spontaneous) fusion was higher, as observed in most other SNARE/Syt fusion studies using reconstitution approaches (Fig. 1e, red trace, adapted from Ref.[19]).

Numerous accounts indicate that the conformations and domain configurations of SNAREs and their regulatory proteins depend on the surrounding lipid bilayer, in which they are embedded [20–24]. The lipid composition also proved to be critically important for fusion of

purified DCVs and reconstituted target membranes. Indeed, Ca^{2+}/Syt1-triggering depended strongly on the amount of phosphatidylinositol-4,5-bisphosphate (PI-4,5-P_2) in the target membrane [19], again reproducing well-established cell physiology [25–28]. Overall, our DCV/supported membrane fusion assay, allows us to uncouple the calcium triggering process from the many other processes that are simultaneously going on in living cells. We therefore sought to correlate a specific SNARE conformation with fusion and to test if the transition from the starting trans-SNARE complex conformation to the fusogenic conformation could be triggered by Ca^{2+}/Syt1. To do so, we measured the tilt angle, i.e., the angle of the nascent SNARE complex relative to the target membrane by site-directed fluorescence-interference contrast (sdFLIC) microscopy (Fig. 1a) under a large variety of fusogenic and non-fusogenic pre- and post-trigger conditions. We found that the nascent SNARE complex moves from a strongly tilted (low tilt angle) to an upright conformation upon Ca^{2+}/Syt1-triggering, presumably induced by a stiffening of the juxta-membrane region of Syx1a that transduces force into the membranes being fused (Fig. 1c and d,). Notably, the size of the tilt angle, which is determined by a key conformational change in the Syx1a hinge region, critically depends on the order of the lipids in the bilayer, in which Syx1a resides. Thus, during fusion, the change in the order of the lipids driven by Ca^{2+}/Syt1 or other means causes Syx1a to assume its fusogenic conformation.

Results

Conformational change of syntaxin in acceptor t-SNARE to cis-SNARE complex transition

A minimal system consisting of a supported membrane that contains only Syx1a and SNAP-25 is capable of fusing with purified DCVs from PC12 cells in a Ca^{2+}-dependent manner (Fig. 1e). In order to observe the different conformations of Syx1a during this process, we employed sdFLIC microscopy, an interferometric technique that measures the absolute distance d_m of a fluorescent tag to the membrane surface [21,29,30] (Fig. 1a, example data for all conditions in Supplementary Figs. 1–3, Supplementary tables 1-2). We prepared three different complexes that each include the Alexa546 label at residue 192 of Syx1a (Syx*192), i.e., the N-terminal end of the SNARE motif and reconstituted them into lipid bilayers composed of porcine brain lipids with head group compositions that mimic the neuronal plasma membrane. The pre-fusion t-SNARE complex is formed in a 1:1 stoichiometry by co-reconstituting Syx*192 with dodecylated SNAP-25 [31]. As found for monomeric Syx1a, the N-terminus of the Syx1a SNARE motif in this acceptor t-SNARE complex is in close proximity to the bilayer surface [21] (first solid bar in Fig. 2a). A post-fusion cis-SNARE complex consisting of Syx*192(183–288) with SNAP-25 and Syb2 that closely resembles the one used by Stein et al. [32] for structure determination by X-ray crystallography was prepared and reconstituted into lipid bilayers of the same composition. As expected from the crystal structure, a measured sdFLIC distance (residue 192 to the membrane surface) of ~10 nm (third solid bar in Fig. 2a) indicates that the cis-SNARE complex stands upright in the membrane. In order to mimic an intermediate trans-SNARE complex, we pre-assembled Syx*192, SNAP-25, and Syb2 lacking the trans membrane domain. Here, residue 192 is about 6 nm from the bilayer surface (second solid bar in Fig. 2a), i.e., intermediate between the distances of the binary t-SNARE and the full cis-SNARE complexes. The results indicate that the juxta-membrane linker region between the SNARE

motif and the transmembrane domain of Syx1a must change its conformation and therefore its secondary structure between the cis and trans complexes.

Ca^{2+}-mediated binding of the C2AB domains of Syt1 to membranes is known to stimulate fusion in vitro [18]. Here, we examine the effects of the Ca^{2+}-mediated translocation of C2AB domains to the membrane on the Syx1a conformation in these SNARE complexes. No changes are detected in the pre-fusion acceptor t-SNARE complex and the post-fusion cis-SNARE complex (first and third open bars in Fig. 2a). However, the trans-SNARE mimicking complex straightens upon C2AB binding and its conformation resembles that of the cis-SNARE complex. Repeating these measurements with the fluorescent label at residue 249 of Syx1a confirmed the C2AB-induced transition from a tilted to the upright conformation (Supplementary Fig. 4a). While the resolution of sdFLIC is not high enough to draw conclusions about the secondary structure of the SNARE complex in the intermediate state, the measured heights of the two residues with respect to the membrane in the final state are consistent with the crystal structure of the cis-SNARE complex [32]. The same conformational change is observed by measuring the distance of Syb1–96, labeled at residue 28, after it has been added to a reconstituted pre-assembled binary complex of Syx1a and SNAP-25 (Supplementary Fig. 4b). It is important to note that, when measured by FLIC, the lipid bilayer surface doesn't change its average distance from the substrate (Supplementary Fig. 4d), something that would be expected if C2AB would induce topographic undulations in the supported membrane. A minor structural change of the SNARE complex is detected when C2AB binds to the membrane in the absence of Ca^{2+}, and the Ca^{2+}/C2AB-induced change is reversible when the sample is washed with EDTA-containing buffer (Supplementary Fig. 4e).

Because Ca^{2+}-dependent vesicle fusion probabilities rely upon the presence of anionic lipids in the target membrane [19], we wanted to know if and how different lipid headgroups alter the conformations of the trans-SNARE complex-mimicking construct. Indeed, only in the presence of anionic lipids, phosphatidylserine (PS) and PI-4,5-P_2, does the SNARE complex change its orientation from a flexible membrane-apposed conformation to a stiff upright conformation upon addition of Ca^{2+}/C2AB (Fig. 2b, Supplementary Fig. 4b). Addition of 15 mol% PS to otherwise uncharged lipids increases the tilt angle of the SNARE complex slightly even in the absence of Ca^{2+}. Adding Ca^{2+}/C2AB further straightens the complex in the presence of PS, but not in a neutral bilayer composed of only phosphatidylcholine (PC), phosphatidylethanolamine (PE), and cholesterol. Adding 1 mol% PI-4,5-P_2 to the PS-containing membrane renders the complex slightly more tilted at PS concentrations below 15 mol% (Supplementary Fig. 4c). Adding additional factors like Munc18 and complexin, does not alter the observed transition into an upright conformation (Supplementary Fig. 4f).

Correlation of Syt C2AB-induced tilt of trans-SNARE mimicking complex with its ability to promote fusion

To test the hypothesis that the changes in SNARE tilt occurring in the absence of vesicle membrane (Fig. 1c) are relevant to fusion, we correlated our distance changes for the trans-SNARE mimicking complex to the fusion probabilities of Syt-deficient DCVs (depleted by shRNA knockdown; SytKD-DCVs) [19] to planar supported target membranes with identical

composition. In the absence of Ca^{2+} (presence of 100 μM EDTA), 23% of all docked DCVs fuse with the Syx/SNAP-25-containing membrane (Fig. 2d). Without Syt, the fusion probability does not increase after the EDTA-containing buffer has been exchanged with 100 μM Ca^{2+} buffer. Adding Ca^{2+} likewise does not change the distance of Syx*192 from the membrane surface (Fig. 2c). However, adding increasing amounts of C2AB dramatically increases both Syx*192-membrane distance and fusion of DCVs. The correlation between our distance measurements and fusion proved to be striking (Fig. 2 c and d, Supplementary tables 2-4). The fusion probability saturates at 0.4 μM C2AB and produces the same level of fusion as wildtype DCVs in 100 μM Ca^{2+}.

Membrane fatty acyl chain composition modulates SNARE conformation and fusion activity

It is known that binding, especially Ca^{2+}-dependent binding, of Syt C2AB to negatively charged membranes containing PI-4,5-P_2 modulates the acyl-chain order of the lipid bilayer [33]. To determine whether lipid chain order contributes to the mechanism by which Syt alters SNARE conformation, we tested phospholipid compositions having a range of different acyl chains and measured SNARE conformation in the absence of Ca^{2+} and C2AB. The trans-SNARE-mimicking complex was reconstituted in four different bilayers in which each of the phospholipids shared a specific fatty acyl composition where the most abundant fatty acids of the plasma membrane were represented: only 16:0 (1,2-dipalmitoyl-, DP) lipids with saturated acyl-chains, only 16:0/18:1 (1-palmitoyl-2-oleoyl-, PO) lipids with mixed acyl-chains, only 18:1 (1,2-dioleoyl-, DO) lipids with unsaturated acyl-chains, and the lipids from brain extracts with a broad distribution of different acyl-chains. All bilayers contained 20 mol% cholesterol and were in the fluid phase. For each of these acyl-chain systems we chose three different head group compositions to measure the distance of Syx*192 and thus the tilt angle of the SNARE helical bundle from the bilayer surface (Supplementary Figs. 2–3, Supplementary table 1): PC only (black bars in Fig. 3a), PC and PE (50:30 mol%, magenta bars in Fig. 3a), and a plasma membrane (PM)-mimicking composition consisting of 34 mol % PC, 30 mol% PE, 15 mol% PS, 1 mol% PI-4,5-P_2, and 20 mol% cholesterol (red bars in Fig. 3a). With these preparations, we tested the capacity of Ca^{2+}/C2AB to modulate the SNARE complex conformation (shift to open red bars in Fig. 3a). In the membrane of highest acyl-chain order, i.e., in all-DP lipids, the SNARE complex has a low tilt angle under all conditions and Ca^{2+}/C2AB does not change this (Fig. 3a). In the membrane of the lowest acyl-chain order, i.e., in all-DO lipids, the SNARE complex becomes more upright, especially when the headgroup composition mimics that of the PM (Fig. 3a). As in the DP lipids, the SNARE complex's conformation is not modulated by Ca^{2+} and C2AB. Intermediate tilt angles are observed when either PO- or brain extract lipids are used (Fig. 3a). Under both of these mixed acyl-chain conditions, addition of Ca^{2+}/C2AB increases the tilt angle of the SNARE complex, with a larger dynamic range in the natural brain lipids than in the synthetic PO lipids (transition from solid to open bars in Fig. 3a). These results indicate that the juxta-membrane region of Syx1a changes from a hinged conformation (with low tilt angle) to an upright (cis-SNARE complex-like) conformation upon disordering of the lipid acyl chains.

In order to correlate these results with fusion, we measured the fusion probability of SytKD-DCVs with the four types of membranes in the absence and presence of Ca^{2+}/C2AB. Without Ca^{2+}/C2AB, fusion is low with target membranes that contain only DP lipids and high with target membranes that contain only DO lipids (Fig. 3b, Supplementary table 3). Addition of Ca^{2+}/C2AB increases the fusion probability only slightly in both cases. Mirroring the Syx*192 distance measurements, target membranes composed of PO- or brain lipids show intermediate initial fusion probabilities in the absence of Ca^{2+}/C2AB that increase dramatically when Ca^{2+} and C2AB are added. These results were confirmed by measuring fluorescence dequenching in ensemble fusion assays using Syx1a/SNAP-25-containing proteoliposomes and purified wild-type DCVs with and without Ca^{2+} (Supplementary Fig. 5 a-e).

To illustrate our interpretation of the sdFLIC results as indicators of low- and high fusion competent SNARE conformations, we visualize the correlation between the tilt angles, i.e. fractions of SNAREs in the highly active state, and the fusion probabilities for conditions with identical lipid headgroup conditions (PM) (Fig. 3c and f,). In this graph, the lowest fusion probability is represented by the results from experiments in DP lipids, while the highest fusion probabilities are derived from the results in DO lipids and in brain lipids after Ca^{2+}/C2AB have been added.

Of all the lipid compositions tested so far, the natural brain lipids show the highest dynamic range ± Ca^{2+}/C2AB, and PS lipids appear to be the strongest contributor toward inducing an increase in the tilt angle of the SNARE complex from the membrane surface. To further test how sensitive the SNARE conformation and DCV fusion is to the fatty acyl-chain composition, we substituted the 15 mol% of brain PS in the brain PM mixture by either DPPS, POPS, or DOPS (Fig. 3, d and e). While POPS could almost completely substitute for brain PS, DPPS and DOPS dramatically impair both the change in tilt angle of the SNARE complex and the Ca^{2+}-mediated fusion increase of wild-type DCVs.

Syt1-C2B domain is the main mediator of SNARE's conformational change

To this point, our comparative studies of the SNARE complex's angle of rise and Ca^{2+}-dependent fusion have focused on the C2AB domain of Syt1. When the C2B and C2A domains were each tested alone, we found C2B to be more potent than C2A in inducing the conformational shift of the trans-SNARE mimicking complex reported by Syx*192. Also, C2B is more effective than C2A in stimulating fusion (Fig. 4a and b,) such that ~74% of the fusion increase mediated by Ca^{2+}/C2AB can be attributed to C2B alone. The latter observation is consistent with the proposed central role of the C2B domain in Ca^{2+} regulated fusion [34,35].

The C2B domain contains a polybasic patch of lysines, which has been shown to strongly mediate the binding of C2B to PI-4,5-P_2 [36,37]. Mutating two of these Lys residues to Ala (K326A and K327A, KAKA mutant) within C2AB strongly impairs the change in tilt angle of the SNARE complex in the sdFLIC assay and the DCV fusion efficiency; both the distance of Syx*192 from the bilayer and the extent of DCV fusion are reduced to the levels observed with C2A alone (Fig. 4c and d, Supplementary tables 2 and 3). These observations correlate with the reduced affinity of the KAKA mutant to PI-4,5-P_2-containing membranes

[36], and in agreement, when we omit PI-4,5-P_2 in the supported target membrane, the difference between C2AB wild-type and the KAKA mutant disappears in the sdFLIC assay (Supplementary Fig. 5f).

A complex consisting of the soluble four-helical SNARE bundle and the C2AB domain of Syt1 has been crystallized in the absence of a lipid bilayer [38]. Based on the crystal structure, the authors proposed three functionally relevant interfaces between the SNAREs and C2AB. One of these interfaces implicated a critical role for two Arg residues at the opposite tip of the Ca^{2+}-binding region of the C2B domain. These Args are also known to affect Ca^{2+}-triggering in neuronal exocytosis [38,39]. When we replaced these Arg residues with Gln in C2AB (R398Q, R399Q, RQRQ mutant) and performed sdFLIC and DCV fusion assays, we found that there are only minor effects on the conformational change of the membrane-bound SNARE complex and, importantly, its fusion activity; these effects can be overcome by higher concentrations of C2AB (Fig. 4e and f,Supplementary tables 2 and 3).

Discussion

Our data show that Ca^{2+}-mediated binding of isolated Syt1-C2AB domains to the target membrane induces a conformational change in the membrane-anchored SNARE complex and increases the fusion probability of SytKD-DCVs with acceptor t-SNARE-containing target membranes. Reconstituted SNARE complexes transition from a bent conformation with their SNARE motifs in close proximity to the membrane surface to a more upright, cis-SNARE complex-mimicking conformation in the membrane. This orientation change strictly correlates with the ability of SNAREs to fuse membranes as probed under a wide range of different conditions. The increases of the tilt angle of the SNARE complex and the associated fusion probability of DCVs require the presence of PS and/or PI-4,5-P_2 in the target membrane.

A second very interesting and novel result of this study is that the control of fusion by Ca^{2+}/C2AB can be bypassed by using a majority of lipids with unsaturated fatty acyl chains, which are less ordered than their saturated counterparts (Fig. 3a and b,). Likewise, the transition can be inhibited by a majority of lipids with more ordered, saturated acyl chains. It has been shown that C2AB binding to lipid bilayers, especially C2B binding, de-mixes and disorders phosphatidylserines [33] and is capable of inducing highly curved membrane structures [40,41]. This suggests a new model for Syt-mediated Ca^{2+} triggering of exocytosis, in which the Syt1-C2AB binding to the lipid bilayer disorders the acyl chains and the changed lipid environment consequently induces a conformational change in the juxta-membrane region of the trans-SNARE complex. The structural re-arrangement of this region in the trans-SNARE complex would pull the two membranes together, exert force on the apposed membranes, and initiate fusion (Fig. 5). While the exact interactions that cause this conformational change are still unknown and require further investigation, we speculate that a balance between electrostatic and hydrophobic lipid-protein interactions determine the precise conformations of the region that eventually becomes the two-helical extension of the four-helical SNARE bundle [32]. The results in this study are a starting point for further research to identify the critical residues in the juxta-membrane SNARE regions and that once identified, this model will be tested in different systems. Adding label positions in the

sdFLIC assay and combining this method with distance constraints obtained from other sources should also allow us to more accurately determine the intermediate protein conformations during this process. While this study has focused on the effects that Ca^{2+}/C2AB has on the target membrane, we cannot exclude that this mechanism is more general and also includes the vesicle membrane.

The proposed model of coupling of Ca^{2+}/Syt action with SNARE-mediated fusion through lipid interactions leads to the following important conclusions: First, the lipid composition of the target membrane is critical for function. The strong interaction between PI-4,5-P_2 and Syx1a [42,43] supports a more tilted (low tilt angle) structure of the SNAREs (Supplementary Fig. 4c) and keeps PI-4,5-P_2 enriched at the fusion site where it would guide membrane insertion of Syt1-C2AB near the developing SNARE complex as required in this model [44]. According to our results, the fatty acyl-chain composition of the synaptic membrane, especially the balance between saturated and unsaturated fatty acids of PS, is a crucial component of our proposed mechanism for the regulation of fusion by Ca^{2+}/Syt. This regulation may be further facilitated by lipid bilayers that fluctuate between more ordered and disordered states [45,46].

Second, a mechanism based on modulating the tilt angle and most likely the stiffness of the SNARE complex would require additional (protein-) factors that organize the SNAREs laterally and vertically between the two membranes to direct the force (symmetrically) to the fusion site and to assure their proper orientation with respect to the membrane surface. Munc18, which has been proposed to act as chaperone for initial SNARE interactions, and Munc13, which is essential for vesicle priming, together could fulfill the role of a spatial organizer of active SNARE complexes [35].

Third, the disordering and demixing of the lipid bilayer caused by Syt at the fusion site is most likely a local effect. Interactions between SNAREs and C2 domains [38] and between individual C2 domains [47] could therefore be part of the priming process that optimize the spatial organization for fast triggering.

Fourth, the priming of the fusion machinery is likely not limited to the organization of the protein content but must also include a reorganization of lipids at or close to the fusion site. As observed in this work, C2AB binding in the absence of Ca^{2+} already influences the SNARE conformation. It has been shown that the C2B domain of Munc13 is important for priming and that mutations in this domain change the Ca^{2+} sensitivity of release [48]. It is therefore plausible that the membrane might be primed and conditioned for fusion by a variety of domains contributed by different peripheral proteins. Indeed, complexin acts on SNAREs *and* lipids in the vicinity of SNAREs. In fact, the N- and C-termini of complexin exhibit curvature-dependent binding to liposomes, which potentially allows for communication between the action of Syt on the lipid bilayer, the binding of complexin with the bilayer [22,23,49], and complexin binding to the SNARE complex.

Tuning the local composition and ordering of the lipid bilayer for various fusion processes may occur on different time- and length-scales. For example, the binding of C2 domains and ensuing changes likely happen very quickly as required for the triggering of synaptic vesicle

fusion, whereas slower forms of exocytosis involved in hormone secretion or other intracellular vesicular transport processes may entail less focal and more sustained changes in composition and order, possibly even involving metabolic mechanisms and modulation by second messengers.

In summary, the results presented in this work strongly suggest that the SNARE proteins constitute not only the minimal machinery in constitutive membrane fusion [7] but are also the major fusogens in Ca^{2+}/synaptotagmin-stimulated fusion. The lipid bilayer is the main coupling agent that renders SNAREs sensitive to Ca^{2+}/synaptotagmin stimulation. The properties of select lipid acyl chains and headgroups are crucial for an efficient local coupling of Ca^{2+}/synaptotagmin and SNARE action to ensure rapid content release for intercellular communication.

Online Methods

Materials.

The following materials were purchased and used without further purification: porcine brain L-α-phosphatidylcholine (bPC), porcine brain L-α-phosphatidylethanolamine (bPE), porcine brain L-α-phosphatidylserine (bPS), porcine brain phosphatidylinositol 4,5-bisphosphate (PI-4,5-P_2, PIP2), 1,2-dipalmitoyl-*sn*-glycero-3-phosphocholine (DPPC), 1,2-dipalmitoyl-*sn*-glycero-3-phosphoethanolamine (DPPE), 1,2-dipalmitoyl-*sn*-glycero-3-phospho-L-serine (DPPS), 1-palmitoyl-2-oleoyl-*sn*-glycero-3-phosphocholine (POPC), 1-palmitoyl-2-oleoyl-*sn*-glycero-3-phosphoethanolamine (POPE), 1-palmitoyl-2-oleoyl-*sn*-glycero-3-phospho-L-serine (POPS), 1,2-dioleoyl-*sn*-glycero-3-phosphocholine (DOPC), 1,2-dioleoyl-*sn*-glycero-3-phosphoethanolamine (DOPE), 1,2-dioleoyl-*sn*-glycero-3-phospho-L-serine (DOPS), 1,2-dioleoyl-sn-glycero-3-phosphoethanolamine-N-(lissamine rhodamine B sulfonyl) (Rh-DOPE), and 1,2-dioleoyl-sn-glycero-3-phosphoethanolamine-N-(7-nitro-2–1,3-benzoxadiazol-4-yl) (NBD-DOPE) were from Avanti Polar Lipids (Alabaster, Al); cholesterol, sodium cholate, 2,2’,2’’,2’’’-(ethane-1,2-diyldinitrilo)tetraacetic acid (EDTA), CaCl2 (Ca2+), OptiPrep density gradient medium, sucrose, 3-(N-Morpholino)propanesulfonic acid (MOPS), L-glutamic acid potassium salt monohydrate, potassium acetate, and glycerol were from Sigma (St. Louis, MO); 3-[(3-cholamidopropyl)dimethylammonio]-1-propanesulfonate (CHAPS), and n-dodecylphosphocholine (DPC) were from Anatrace (Maumee, OH); 2-[4-(2-hydroxyethyl)piperazin-1-yl]ethanesulfonic acid (HEPES) was from Research Products International (Mount Prospect, IL); chloroform, ethanol, Contrad detergent, all inorganic acids, bases, and hydrogen peroxide were from Fisher Scientific (Fair Lawn, NJ). Alexa Fluor 546 C5 maleimide was from Thermo Fisher Scientific. Water was purified first with deionizing and organic-free 3 filters (Virginia Water Systems, Richmond, VA) and then with a NANOpure system from Barnstead (Dubuque, IA) to achieve a resistivity of 18.2 MΩ/cm.

Cell line.

Rat pheochromocytoma cells (PC12) were originally obtained from E. Chapman, University of Wisconsin, and routinely tested for mycoplasma.

FLIC substrates.

Previously introduced FLIC substrates with quadratic terraces of 10 × 10 μm and of 16 different oxide thicknesses ranging from 10 to 450 nm thickness were used in all sdFLIC experiments [21]. The fabrication by photolithography and HF etching, was described in detail elsewhere [50,51]. Oxide thicknesses were measured after fabrication by microellipsometry (Accurion Inc.) and checked regularly, using a supported 1-palmitoyl-2-oleoyl-sn-glycero-3-phosphocholine (POPC) membrane prepared by vesicle fusion as the standard experiment [52].

Protein purification and labeling.

Syntaxin-1a (both constructs of residues 183–288 and 1–288, with single cysteine mutation at amino acid position 192), wild-type, cys-free (all 4 cysteines were mutated to serines) SNAP-25, soluble (residues 1–96) and full length synaptobrevin-2, Munc18, and complexin-1 from *Rattus norvegicus* were expressed in *Escherichia coli* strain BL21(DE3) cells under the control of the T7 promoter in the pET28a expression vector and purified as described previously[21,53,24]. Briefly, all proteins were purified using Ni-NTA affinity chromatography. After the removal of N-terminal His-tags by thrombin cleavage, proteins were further purified by subsequent ion-exchange or size-exclusion chromatography when necessary. Wild-type SNAP-25 was quadruply dodecylated through disulfide exchange with dodecyl methanethiosulfonate (Toronto Research Company, Toronto, Ontario) to its 4 native cysteines [31]. This lipid-anchored form of SNAP-25 together with syntaxin-1a was used for reconstituting acceptor complex in membranes, whereas the cys-free SNAP-25 was employed for preassembled SNARE complexes (Supplementary Figures 4 b and c,).

His-tagged syntaxin-1a was reacted with an at least twofold molar excess of Alexa-546 in thoroughly degassed DPC-buffers. Labeled proteins were separated from free dye via extensive wash after re-binding to Ni-NTA column. Subsequently, eluted Alexa-labeled proteins were subjected to thrombin cleavage and then purified by size-exclusion chromatography [21].

The expression and purification of Syt1 C2A (residues 136–260), C2B (residues 262–421), and C2AB constructs (residues 136–421) was carried out as previously published [36,54]. Briefly, Syt1 domains were derived from *Rattis norvegicus* and expressed in pGEX-KG constructs. The native cysteine at residue position 277 was mutated to an alanine. The C2AB construct mutations R398Q/R399Q and K326A/K327A were produced by QuickChange site-directed mutagenesis (Agilent, Santa Clara, CA). The wild-type and mutant plasmids were expressed in BL21(DE3) cells (Invitrogen, Grand Island, NY) and the proteins were purified using GST affinity chromatography. The GST-tag was removed via thrombin-cleavage. Constructs were further purified by ion exchange chromatography to remove additional protein and nucleic acid contaminants. Purity was verified by SDS-Page and UV absorbance (260/280) and protein quantification was based on absorbance at 280 nm.

Reconstitution of SNAREs into proteoliposomes.

All SNARE proteins, acceptor complex and SNARE complexes, were reconstituted using sodium cholate as previously described [55]. The desired lipids were mixed, and organic

solvents were evaporated under a stream of N_2 gas followed by vacuum desiccation for at least 1 hour. The dried lipid films were dissolved in 25 mM sodium cholate in buffer (20 mM HEPES, 150 mM KCl, pH 7.4) followed by the addition of an appropriate volume of the desired SNARE protein(s) in their respective detergents to reach a final lipid/protein ratio of 4000 for each protein. After 1 hour of equilibration at room temperature, the mixture was diluted to reach a sodium cholate concentration of 16 mM, close to the critical micellar concentration, by adding more buffer to the desired final volume. The sample was then dialyzed overnight against 1 L of buffer with 1 buffer change after ~4 hours. The exact lipid compositions of all experiments are listed in the Supplementary tables 1-4.

Preparation of planar supported bilayers containing SNARE complexes.

Planar supported bilayers with reconstituted plasma membrane SNAREs were prepared by the Langmuir-Blodgett/vesicle fusion technique as described in previous studies [42,56,57]. FLIC chips or quartz slides were cleaned by dipping in 3:1 sulfuric acid: hydrogen peroxide for 15 minutes using a Teflon holder. Slides were then rinsed thoroughly in water. The first leaflet of the bilayer was prepared by Langumir-Blodgett transfer directly onto the quartz slide using a Nima 611 Langmuir-Blodgett trough (Nima, Conventry, UK) by applying the lipid mixture of 80:20:3 PC:Chol:DPS from a chloroform solution using PC acyl chains to match the conditions indicated in the text. After allowing the solvent to evaporate for 10 minutes, the monolayer was compressed at a rate of 10 cm^2/minute to reach a surface pressure of 31 mN/m. After equilibration for 5 to 10 minutes, a clean quartz slide was rapidly (200 mm/minute) dipped into the trough and slowly (5 mm/minute) withdrawn, while a computer maintained a constant surface pressure and monitored the transfer of lipids with head groups down onto the hydrophilic substrate. Proteoliposomes were incubated with the Langmuir-Blodgett monolayer to form the outer leaflet of the planar supported bilayer. A concentration of 77 – 90 mM total lipid in 1.1 – 1.3 mL total volume was used. After incubation of the proteoliposomes for 2 hours the excess proteoliposomes were removed by perfusion with 10 mL of buffer (120 mM potassium glutamate, 20 mM potassium acetate, 20 mM HEPES, pH 7.4 for DCV fusion experiments or 150 mM KCl, 20mM HEPES, pH 7.4 for sdFLIC experiments). During the experiments buffers were exchanged with buffers that contained either 100 μM $CaCl_2$ or 100 μM EDTA in addition to the above compositions.

Plasmids and shRNA constructs.

Plasmids and shRNA constructs used for preparations of DCVs have been previously described [19]. For simultaneous shRNA knockdown of multiple syt isoforms, a modified pLKO.5 vector containing shRNA expression cassettes targeting syt1 (TRCN0000093258) and syt9 (TRCN0000379591) from Mission shRNA plasmids (Sigma-Aldrich) was used.

Cell culture.

Wild-type pheochromocytoma cells (PC12) and a PC12 cell line stably expressing a syt1-syt9 double knock-down shRNA cassette were cultured as previously described [19] on 10 cm plastic cell culture plates at 37ºC in 10% CO_2 in Dulbecco's Modified Eagle Medium (DMEM) High Glucose 1 X Gibco supplemented with 10% horse serum (Cellgro),10% calf serum (Fe^+) (Hyclone), and 1% penicillin/streptomycin mix. Medium was changed every 2–3 days and cells were passaged after reaching 90% confluency by incubating 5 min in HBSS

and replating in fresh medium. Cells were transfected with NPY-Ruby by electroporation using an Electro Square Porator ECM 830 (BTX). After harvesting and sedimentation, cells were suspended in a small volume of sterile cytomix electroporation buffer [58] (120 mM KCl, 10 mM KH_2PO_4, 0.15 mM $CaCl_2$, 2 mM EGTA, 25 mM HEPES-KOH, 5 mM $MgCl_2$, 2 mM ATP, and 5 mM glutathione, pH 7.6) and then counted and diluted to ~14×10^6 cells/mL. 700 μL of cell suspension (~10×10^6 cells) and 30 μg of DNA were placed in an electroporator cuvette with 4 mm gap and two 255V, 8 ms electroporation pulses were applied. Cells were then transferred to a 10 cm cell culture dish with 10 mL of normal growth medium. NPY-Ruby transfected cells were cultured under normal conditions for 3 days after transfection and then used for fractionation.

DCV purification.

DCVs were purified using iso-osmotic media as previously described [19]. PC12 cells (15–30 10-cm plates depending on experiments) were scraped into PBS, pelleted by centrifugation, resuspended and washed once in homogenization medium (0.26 M sucrose, 5 mM MOPS, and 0.2 mM EDTA). Following resuspension in (3 ml) homogenization medium containing protease inhibitor (Roche Diagnostics), the cells were cracked open using a ball bearing homogenizer with a 0.2507-inch bore and 0.2496-inch diameter ball. The homogenate was then spun at 4000 rpm (1000 × g), 10 min at 4°C in fixed-angle microcentrifuge to pellet nuclei and larger debris. The postnuclear supernatant (PNS) was collected and spun at 11,000 rpm (8000 × g), 15 min at 4°C to pellet mitochondria. The postmitochondrial supernatant (PMS) was then collected, adjusted to 5 mM EDTA, and incubated 10 min on ice. A working solution of 50% Optiprep (iodixanol) (5 vol 60% Optiprep: 1 vol 0.26M sucrose, 30 mM MOPS, 1 mM EDTA) and homogenization medium were mixed to prepare solutions for discontinuous gradients in Beckman SW55 tubes: 0.5 mL of 30% iodixanol on the bottom and 3.8 mL of 14.5% iodixanol, above which 1.2 ml EDTA-adjusted PMS was layered. Samples were spun at 45,000 rpm (190,000 × g) for 5 h. A clear white band at the interface between the 30% iodixanol and the 14.5% iodixanol was collected as the DCV sample. The DCV sample was then extensively dialyzed (2–3 buffer changes) in a cassette with 10,000 kD molecular weight cutoff (24–48 h, 3 × 5L) into the fusion assay buffer (120 mM potassium glutamate, 20 mM potassium acetate, 20 mM HEPES, pH 7.4).

Site-directed fluorescence interference contrast (sd-FLIC) microscopy.

The principle of site-directed fluorescence interference contrast (FLIC) microscopy and the set up as used in this work, has been described previously [21]. A membrane containing protein with specifically labeled cysteines is supported on a patterned silicon chip with microscopic steps of silicon dioxide. The fluorescence intensity depends on the position of the dye with respect to the standing modes of the exciting and emitting light in front of the reflecting silicon surface. The position is determined by the variable-height 16 oxide steps and the constant average distance between dye and silicon oxide [58].

Images were acquired on a Zeiss Axiovert 200 or Axio Observer 7 fluorescence microscope (Carl Zeiss) with a mercury lamp as a light source and a 40× water immersion objective (Zeiss; N.A. = 0.7). Fluorescence was observed through a 610-nm band-pass filter (D610/60; Chroma) by a CCD camera (DV-887ESC-BV; Andor-Technologies). Exposure times for

imaging were set between 40 and 80 ms, and the excitation light was filtered by a neutral density filter (ND 1.0, Chroma) to avoid photobleaching.

During sdFLIC experiments, we acquired 4–6 images, 20–30 min after buffer changes, for each membrane condition of one supported membrane. From each image, we extracted 100 sets of 16 fluorescence intensities and fitted the optical theory with the fluorophore-membrane distance as fit parameter. Software to fit the data was kindly provided by the authors of [58]. The standard deviation of these ~400–600 results were usually in the order of 1 nm (see Supplemental Figures 1–3 for raw data). The optical model consists of 5 layers of different thickness and refractive indices (bulk silicon, variable silicon oxide, 4 nm water, 4 nm membrane, bulk water), which we kept constant for all conditions [21,29,52]. The reported errors for the absolute membrane distance of each protein and lipid condition in EDTA are the standard errors from at least 3 repeats (see Supplemental tables 1 and 2 for statistics). Not included in these errors are systematic errors that might origin in different membrane thicknesses or membrane-substrate distances between different lipid conditions and a systematic underestimation of the residue-membrane distance from 10–20% of protein that is trapped on the substrate proximal side of the supported bilayer. The reported errors after buffer changes or the addition of C2AB are the standard errors of the detected distance changes from at least 3 repeats for each condition. Based on previous experiments with polymer supported bilayers we estimate the systematic uncertainty for the measured absolute distance to be ~1–2 nm [52]. The systematic underestimation of the real distance caused by protein trapped on the substrate side of the supported membrane can be estimated if we assume that 10% of fluorophores reside at an average position between oxide surface and membrane [21], i.e. at −6 nm from the distal membrane surface. With this assumption measured FLIC distances of 0 nm, 5 nm and 10 nm would originate from 90 % fluorophores at 0.7 nm, 6.2 nm and 11.8 nm. Note, that when the labeled protein is added as a ligand to the membrane, as is the case for Syb*28(1–96) in Supplemental Figure 4, all fluorophores are on the distal site of the membrane.

Total internal reflection fluorescence (TIRF) microscopy.

Experiments examining single-vesicle docking and fusion events were performed on a Zeiss Axiovert 35 fluorescence microscope (Carl Zeiss, Thornwood, NY), equipped with a 63x water immersion objective (Zeiss; N.A. = 0.95) and a prism-based TIRF illumination. The light source was an OBIS 532 LS laser from Coherent Inc. (Santa Clara Ca.). Fluorescence was observed through a 610 nm band pass filter (D610/60; Chroma, Battleboro, VT) by an electron multiplying CCD (DU-860E; Andor Technologies). The prism-quartz interface was lubricated with glycerol to allow easy translocation of the sample cell on the microscope stage. The beam was totally internally reflected at an angle of 72^{o} from the surface normal, resulting in an evanescent wave that decays exponentially with a characteristic penetration depth of ~100 nm. An elliptical area of 250 × 65 μm was illuminated. The laser intensity, shutter, and camera were controlled by a homemade program written in LabVIEW (National Instruments, Austin, TX).

Experiments triggering DCV fusion with calcium were done on a Zeiss Axiovert 200 fluorescence microscope (Carl Zeiss, Thornwood, NY), with objective and TIRF set ups as

described above. The light source was a 514 nm beam line of an argon ion laser (Innova 90C, Coherent, Palo Alto, CA), controlled through an acousto-optic modulator (Isomet, Springfield, VA), and a diode laser (Cube 640, Coherent) emitting light at 640 nm. The characteristic penetration depth was ~102 nm and ~130 nm for the 514 and 640 nm lasers, respectively. An OptoSplit (Andor-Technologies, South Windsor, CT) was used to separate the fluorescence from the NPY-Ruby and Cy5 fluorescence. Fluorescence signals were recorded by an electron-multiplying charge-coupled device camera (iXon DV887ESC-BV, Andor, Belfast, UK).

Single DCV fusion assay.

Acceptor t-SNARE protein containing planar supported bilayers were washed with fusion buffer containing EDTA or divalent metal Ca^{2+} as indicated in text. They were then perfused with DCV (50–100 μL depending on preparation) diluted into 2 mL of fusion buffer (120 mM potassium glutamate, 20 mM potassium acetate, 20 mM HEPES, pH 7.4) with additions of EDTA, or Ca^{2+}/C2 as indicated in text. In experiments with Munc18 and/or complexin, the supported membrane was incubated with 0.5 μM Munc18 and/or 2 μM complexin, 15 min before DCVs were added and the same amount of protein was added to the DCV solution to keep the concentrations constant throughout the experiment. The fluorescence from DCVs was recorded by exciting with the 532 nm laser and using a EMCCD camera. After injection of the DCV sample, the microscope was focused within no more than 30 seconds and then a total of 5000 images were taken with 200 ms exposure times and spooled directly to the hard drive.

Single-vesicle fusion data were analyzed using a homemade program written in LabView (National Instruments). Stacks of images were filtered by a moving average filter. The maximum intensity for each pixel over the whole stack was projected on a single image. Vesicles were located in this image by a single-particle detection algorithm described in [59]. The peak (central pixel) and mean fluorescence intensities of a 5 × 5 $pixel^2$ area around each identified center of mass were plotted as a function of time for all particles in the image series. The fusion efficiency was determined from the number of vesicles that underwent fusion within 15 s after they docked relative to the total number of vesicles that docked. Results are reported as mean ± standard errors from 5 repeats of the experiments (see Supplemental tables 3 and 4 for statistics).

Ensemble DCV lipid mixing assay.

Proteoliposomes containing t-SNAREs (syntaxin-1 and SNAP-25) with FRET paired lipid probes (1.5 % each of Rh-DOPE and NBD-DOPE) were incubated at 37 ^{o}C in fusion buffer (120 mM potassium glutamate, 20 mM potassium acetate, 20 mM HEPES, pH 7.4) with either 100 μM EDTA or 100 μM Ca^{2+}. After 10 minutes of incubation fluorimeter recording was started and DCVs (25–50 μL) were added and NBD-dequenching was monitored. Experiments were repeated 3 times. The average fluorescence increase is reported as mean +/− standard deviation.

Data availability.

The data that support the findings of this study are available from the corresponding author on reasonable request.

Custom code availability.

The custom code used to acquire and analyze the data in this study is available from the corresponding author on reasonable request.

Supplementary Material

Refer to Web version on PubMed Central for supplementary material.

Acknowledgments:

We thank A. Lambacher and P. Fromherz for providing FLIC analysis software and for their help with the production of FLIC substrates.

NIH Grant P01 GM72694: L.K.T., D.S.C, B.L., and V.K.

References

1. Sabatini BL & Regehr WG Timing of neurotransmission at fast synapses in the mammalian brain. Nature 384, 170–172, doi:10.1038/384170a0 (1996). [PubMed: 8906792]
2. Schneggenburger R & Neher E Intracellular calcium dependence of transmitter release rates at a fast central synapse. Nature 406, 889–893, doi:10.1038/35022702 (2000). [PubMed: 10972290]
3. Sudhof TC Neurotransmitter release: the last millisecond in the life of a synaptic vesicle. Neuron 80, 675–690, doi:10.1016/j.neuron.2013.10.022 (2013). [PubMed: 24183019]
4. Sudhof TC A molecular machine for neurotransmitter release: synaptotagmin and beyond. Nat Med 19, 1227–1231, doi:10.1038/nm.3338 (2013). [PubMed: 24100992]
5. Jahn R & Fasshauer D Molecular machines governing exocytosis of synaptic vesicles. Nature 490, 201–207, doi:10.1038/nature11320 (2012). [PubMed: 23060190]
6. Jahn R & Scheller RH SNAREs - engines for membrane fusion. Nat. Rev. Mol. Cell Biol 7, 631–643 (2006). [PubMed: 16912714]
7. Weber T et al. SNAREpins: Minimal machinery for membrane fusion. Cell 92, 759–772 (1998). [PubMed: 9529252]
8. Geppert M et al. Synaptotagmin-I - a Major Ca2+ Sensor for Transmitter Release at a Central Synapse. Cell 79, 717–727, doi:10.1016/0092-8674(94)90556-8 (1994). [PubMed: 7954835]
9. Stein A, Radhakrishnan A, Riedel D, Fasshauer D & Jahn R Synaptotagmin activates membrane fusion through a Ca2+-dependent trans interaction with phospholipids. Nat Struct Mol Biol 14, 904–911, doi:10.1038/nsmb1305 (2007). [PubMed: 17891149]
10. Kiessling V et al. Rapid fusion of synaptic vesicles with reconstituted target SNARE membranes. Biophys J 104, 1950–1958, doi:10.1016/j.bpj.2013.03.038 (2013). [PubMed: 23663838]
11. Kyoung M, Zhang Y, Diao J, Chu S & Brunger AT Studying calcium-triggered vesicle fusion in a single vesicle-vesicle content and lipid-mixing system. Nature protocols 8, 1–16, doi:10.1038/nprot.2012.134 (2013). [PubMed: 23222454]
12. Lee HK et al. Dynamic Ca2+-dependent stimulation of vesicle fusion by membrane-anchored synaptotagmin 1. Science 328, 760–763, doi:10.1126/science.1187722 (2010). [PubMed: 20448186]
13. Tucker WC, Weber T & Chapman ER Reconstitution of Ca2+-Regulated Membrane Fusion by Synaptotagmin and SNAREs. Science 304, 435–438 (2004). [PubMed: 15044754]
14. Malsam J et al. Complexin arrests a pool of docked vesicles for fast Ca2+-dependent release. The EMBO journal 31, 3270–3281, doi:10.1038/emboj.2012.164 (2012). [PubMed: 22705946]

15. Sudhof TC & Rothman JE Membrane Fusion: Grappling with SNARE and SM Proteins. Science 323, 474–477, doi:10.1126/science.1161748 (2009). [PubMed: 19164740]
16. Rizo J & Xu J The Synaptic Vesicle Release Machinery. Annu Rev Biophys 44, 339–367, doi:10.1146/annurev-biophys-060414-034057 (2015). [PubMed: 26098518]
17. Ledesma MD, Martin MG & Dotti CG Lipid changes in the aged brain: effect on synaptic function and neuronal survival. Prog Lipid Res 51, 23–35, doi:10.1016/j.plipres.2011.11.004 (2012). [PubMed: 22142854]
18. Ma C, Su L, Seven AB, Xu Y & Rizo J Reconstitution of the vital functions of Munc18 and Munc13 in neurotransmitter release. Science 339, 421–425, doi:10.1126/science.1230473 (2013). [PubMed: 23258414]
19. Kreutzberger AJB et al. Reconstitution of calcium-mediated exocytosis of dense-core vesicles. Sci Adv 3, e1603208, doi:10.1126/sciadv.1603208 (2017). [PubMed: 28776026]
20. Liang B, Dawidowski D, Ellena JF, Tamm LK & Cafiso DS The SNARE motif of synaptobrevin exhibits an aqueous-interfacial partitioning that is modulated by membrane curvature. Biochemistry 53, 1485–1494, doi:10.1021/bi401638u (2014). [PubMed: 24552121]
21. Liang B, Kiessling V & Tamm LK Prefusion structure of syntaxin-1A suggests pathway for folding into neuronal trans-SNARE complex fusion intermediate. Proc Natl Acad Sci U S A 110, 19384–19389, doi:10.1073/pnas.1314699110 (2013). [PubMed: 24218570]
22. Zdanowicz R et al. Complexin Binding to Membranes and Acceptor t-SNAREs Explains Its Clamping Effect on Fusion. Biophys J 113, 1235–1250, doi:10.1016/j.bpj.2017.04.002 (2017). [PubMed: 28456331]
23. Gong J et al. C-terminal domain of mammalian complexin-1 localizes to highly curved membranes. Proc Natl Acad Sci U S A 113, E7590–E7599, doi:10.1073/pnas.1609917113 (2016). [PubMed: 27821736]
24. Dawidowski D & Cafiso DS Allosteric control of syntaxin 1a by Munc18–1: characterization of the open and closed conformations of syntaxin. Biophys J 104, 1585–1594, doi:10.1016/j.bpj.2013.02.004 (2013). [PubMed: 23561535]
25. Cremona O & De Camilli P Phosphoinositides in membrane traffic at the synapse. J Cell Sci 114, 1041–1052 (2001). [PubMed: 11228149]
26. Holz RW & Axelrod D Localization of phosphatidylinositol 4,5-P(2) important in exocytosis and a quantitative analysis of chromaffin granule motion adjacent to the plasma membrane. Ann N Y Acad Sci 971, 232–243 (2002). [PubMed: 12438123]
27. Milosevic I et al. Plasmalemmal phosphatidylinositol-4,5-bisphosphate level regulates the releasable vesicle pool size in chromaffin cells. J Neurosci 25, 2557–2565, doi:10.1523/JNEUROSCI.3761-04.2005 (2005). [PubMed: 15758165]
28. Martin TF Role of PI(4,5)P(2) in vesicle exocytosis and membrane fusion. Subcell Biochem 59, 111–130, doi:10.1007/978-94-007-3015-1_4 (2012). [PubMed: 22374089]
29. Kiessling V & Tamm LK Measuring distances in supported bilayers by fluorescence interference-contrast microscopy: polymer supports and SNARE proteins. Biophys J 84, 408–418 (2003). [PubMed: 12524294]
30. Lambacher A & Fromherz P Luminescence of dye moleculars on oxidized silicon and fluorescence interference contrast (FLIC) microscopy of biomembranes. J. Opt. Soc. Am. B 19, 1435–1453 (2002).
31. Kreutzberger AJ, Liang B, Kiessling V & Tamm LK Assembly and comparison of plasma membrane SNARE acceptor complexes. Biophys J 110, 2147–2150, doi:10.1016/j.bpj.2016.04.011 (2016). [PubMed: 27178662]
32. Stein A, Weber G, Wahl MC & Jahn R Helical extension of the neuronal SNARE complex into the membrane couples zippering to membrane fusion. Nature 460, 525–528, doi:10.1038/nature08156 (2009). [PubMed: 19571812]
33. Lai AL, Tamm LK, Ellena JF & Cafiso DS Synaptotagmin 1 modulates lipid acyl chain order in lipid bilayers by demixing phosphatidylserine. J Biol Chem 286, 25291–25300, doi:10.1074/jbc.M111.258848 (2011). [PubMed: 21610074]

34. Gaffaney JD, Dunning FM, Wang Z, Hui E & Chapman ER Synaptotagmin C2B domain regulates Ca2+-triggered fusion in vitro: critical residues revealed by scanning alanine mutagenesis. J Biol Chem 283, 31763–31775, doi:10.1074/jbc.M803355200 (2008). [PubMed: 18784080]
35. Rizo J & Rosenmund C Synaptic vesicle fusion. Nat. Struct. Molec. Biol 15, 665–674 (2008). [PubMed: 18618940]
36. Perez-Lara A et al. PtdInsP2 and PtdSer cooperate to trap synaptotagmin-1 to the plasma membrane in the presence of calcium. eLife 5, doi:10.7554/eLife.15886 (2016).
37. Park Y et al. Synaptotagmin-1 binds to PIP(2)-containing membrane but not to SNAREs at physiological ionic strength. Nat Struct Mol Biol 22, 815–823, doi:10.1038/nsmb.3097 (2015). [PubMed: 26389740]
38. Zhou Q et al. Architecture of the synaptotagmin-SNARE machinery for neuronal exocytosis. Nature 525, 62–67, doi:10.1038/nature14975 (2015). [PubMed: 26280336]
39. Wang S, Li Y & Ma C Synaptotagmin-1 C2B domain interacts simultaneously with SNAREs and membranes to promote membrane fusion. eLife 5, doi:10.7554/eLife.14211 (2016).
40. McMahon HT, Kozlov MM & Martens S Membrane curvature in synaptic vesicle fusion and beyond. Cell 140, 601–605, doi:10.1016/j.cell.2010.02.017 (2010). [PubMed: 20211126]
41. Hui E, Johnson CP, Yao J, Dunning FM & Chapman ER Synaptotagmin-mediated bending of the target membrane is a critical step in Ca(2+)-regulated fusion. Cell 138, 709–721, doi:10.1016/j.cell.2009.05.049 (2009). [PubMed: 19703397]
42. Wagner ML & Tamm LK Reconstituted syntaxin1A/SNAP25 interacts with negatively charged lipids as measured by lateral diffusion in planar supported bilayers. Biophys J 81, 266–275 (2001). [PubMed: 11423412]
43. van den Bogaart G et al. Membrane protein sequestering by ionic protein-lipid interactions. Nature 479, 552–555, doi:10.1038/nature10545 (2011). [PubMed: 22020284]
44. Honigmann A et al. Phosphatidylinositol 4,5-bisphosphate clusters act as molecular beacons for vesicle recruitment. Nat Struct Mol Biol 20, 679–686, doi:10.1038/nsmb.2570 (2013). [PubMed: 23665582]
45. Simons K & Ikonen E Functional rafts in cell membranes. Nature 387, 569–572 (1997). [PubMed: 9177342]
46. Veatch SL et al. Critical fluctuations in plasma membrane vesicles. ACS Chem Biol 3, 287–293, doi:10.1021/cb800012x (2008). [PubMed: 18484709]
47. Wang J et al. Calcium sensitive ring-like oligomers formed by synaptotagmin. Proc Natl Acad Sci U S A 111, 13966–13971, doi:10.1073/pnas.1415849111 (2014). [PubMed: 25201968]
48. Shin OH et al. Munc13 C2B domain is an activity-dependent Ca2+ regulator of synaptic exocytosis. Nat Struct Mol Biol 17, 280–288, doi:10.1038/nsmb.1758 (2010). [PubMed: 20154707]
49. Snead D, Wragg RT, Dittman JS & Eliezer D Membrane curvature sensing by the C-terminal domain of complexin. Nature communications 5, 4955, doi:10.1038/ncomms5955 (2014).

Methods-only References

50. Braun D & Fromherz P Fluorescence interferometry of neuronal cell adhesion on microstructured silicon. Phys. Rev. Letters 81, 5241–5244 (1998).
51. Braun D & Fromherz P Fluorescence interference-contrast microscopy of cell adhesion on oxidized silicon. Appl Phys A 65, 341–348 (1997).
52. Crane JM, Kiessling V & Tamm LK Measuring lipid asymmetry in planar supported lipid bilayers by fluorescence interference contrast microscopy. Biophys J 88, 234A–234A (2005).
53. Pabst S et al. Selective interaction of complexin with the neuronal SNARE complex - Determination of the binding regions. J.Biol.Chem 275, 19808–19818 (2000). [PubMed: 10777504]
54. Katti S et al. Non-Native Metal Ion Reveals the Role of Electrostatics in Synaptotagmin 1-Membrane Interactions. Biochemistry 56, 3283–3295, doi:10.1021/acs.biochem.7b00188 (2017). [PubMed: 28574251]

55. Domanska MK, Kiessling V, Stein A, Fasshauer D & Tamm LK Single vesicle millisecond fusion kinetics reveals number of SNARE complexes optimal for fast SNARE-mediated membrane fusion. J Biol Chem 284, 32158–32166, doi:10.1074/jbc.M109.047381 (2009). [PubMed: 19759010]

56. Wagner ML & Tamm LK Tethered polymer-supported planar lipid bilayers for reconstitution of integral membrane proteins: Silane-polyethyleneglycol-lipid as a cushion and covalent linker. Biophys J 79, 1400–1414 (2000). [PubMed: 10969002]

57. Kalb E, Frey S & Tamm LK Formation of supported planar bilayers by fusion of vesicles to supported phospholipid monolayers. Biochim Biophys Acta 1103, 307–316 (1992). [PubMed: 1311950]

58. van den Ent F & RF Lowe, J. cloning: a restriction-free method for inserting target genes into plasmids. J Biochem Biophys Methods 67, 67–74, doi:10.1016/j.jbbm.2005.12.008 (2006). [PubMed: 16480772]

59. Kiessling V, Crane JM & Tamm LK Transbilayer effects of raft-like lipid domains in asymmetric planar bilayers measured by single molecule tracking. Biophys J 91, 3313–3326, doi:10.1529/biophysj.106.091421 (2006). [PubMed: 16905614]

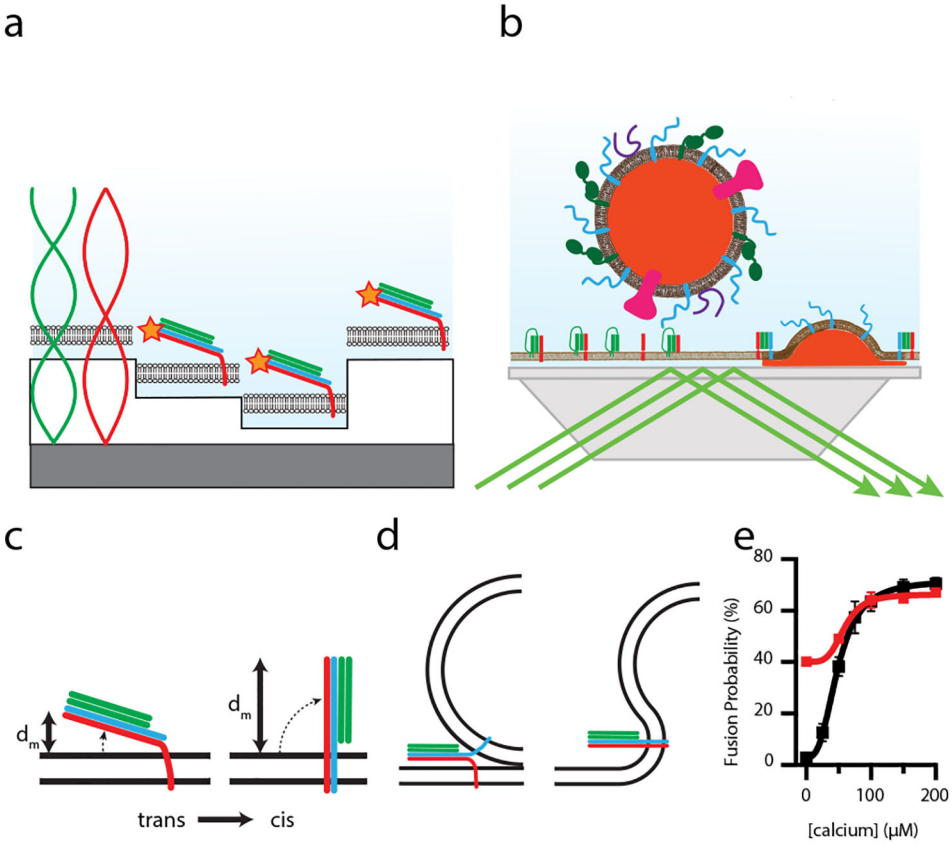

Fig. 1. Correlating conformational changes in SNARE proteins with fusion efficiency during Ca^{2+} triggered vesicle fusion.

a, Distance measurements by sdFLIC microscopy. A supported membrane containing protein complexes with specifically labeled cysteines is prepared on a Si/SiO_2 substrate with different steps. Fluorescent images of the planar membrane are used to probe the interference pattern originating from reflected excitation and emission light in order to determine the distance of the fluorophores from the lipid bilayer surface. **b**, Single DCV fusion TIRF assay. Fluorescence originating from NPY-Ruby of single vesicles can be imaged when they enter the evanescent field of a TIRF microscope. Characteristic intensity traces from docking and fusion events of vesicles with SNARE containing supported membranes are analyzed to determine docking and fusion probabilities. **c**,**d**, Syx*192-membrane distance d_M as measured by sdFLIC microscopy in a trans-mimicking SNARE complex lacking the Syb transmembrane domain (left) and a cis-SNARE complex (c), and the hypothesized corresponding trans and cis steps in vesicle fusion (d). **e**, Fusion probability of purified DCVs with Syx1a/SNAP-25-containing supported membranes as a function of Ca^{2+} concentration in the buffer. Fusion is either triggered from a docked state by the addition of Ca^{2+} in the presence of Munc18 and complexin-1 (black) or is observed directly after docking in a minimal (SNARE-only) system lacking all regulatory proteins on the supported membrane (red). Data are replotted from Kreutzberger et al. 2017 [19].

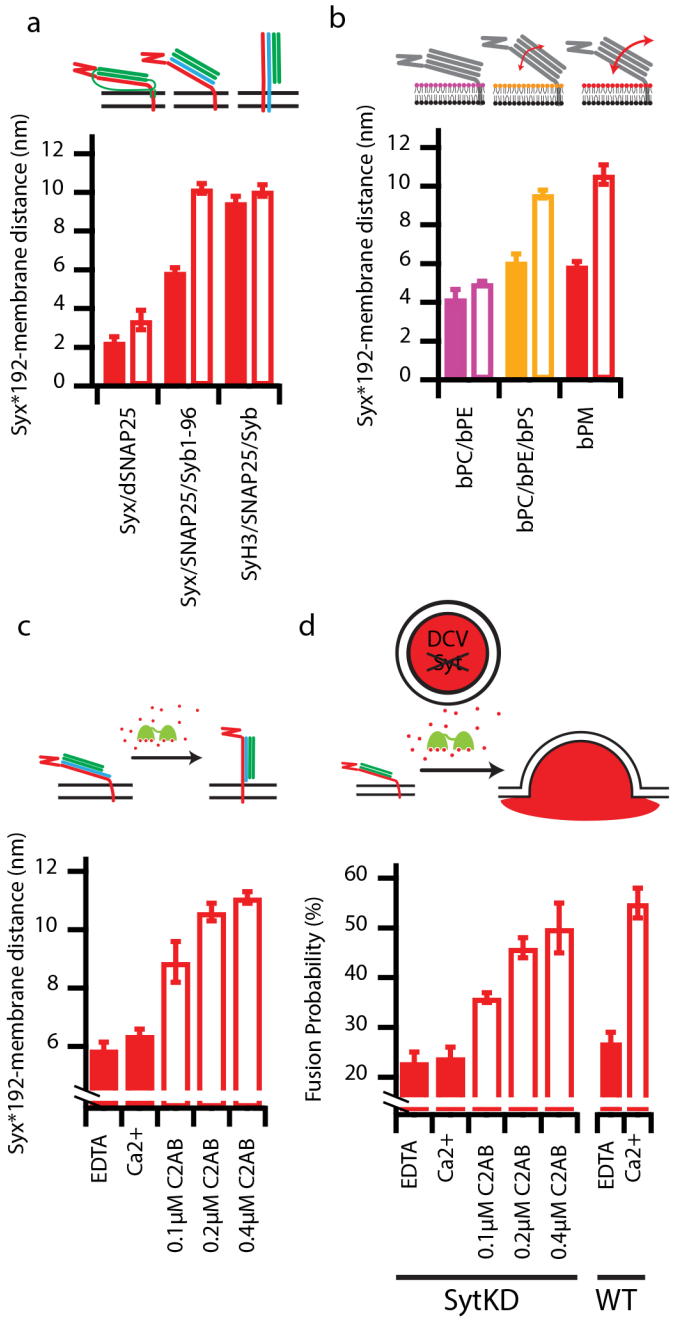

Fig. 2. C2AB induces trans-cis conformational transition of neuronal SNARE complex.

a, Syx*192-membrane distance in three different SNARE complexes in a plasma membrane-mimicking bilayer before (solid bars) and after the addition of Ca^{2+} and C2AB. **b**, Syx*192-membrane distance in the trans-mimicking SNARE complex in three different lipid headgroup environments (magenta: bPC/bPE/cholesterol, 5/3/2; orange: bPC/bPE/bPS/cholesterol, 3.5/3/1.5/2; red: bPM, i.e. bPC/bPE/bPS/bPIP2/cholesterol, 3.4/3/1.5/0.1/2) before (solid bars) and after the addition of Ca^{2+} and C2AB (open bars). **c**, Syx*192-membrane distance upon Ca^{2+}/C2AB titration showing a transition from a trans-like SNARE complex to a cis-like SNARE complex. **d**, Fusion probability of SytKD-DCVs upon Ca^{2+}/

C2AB titration and of wild-type DCVs in the presence and absence of Ca^{2+}. All data represent means from at least 5 independent experiments (see Supplemental tables 1–4 for details). Error bars represent s.e.m.

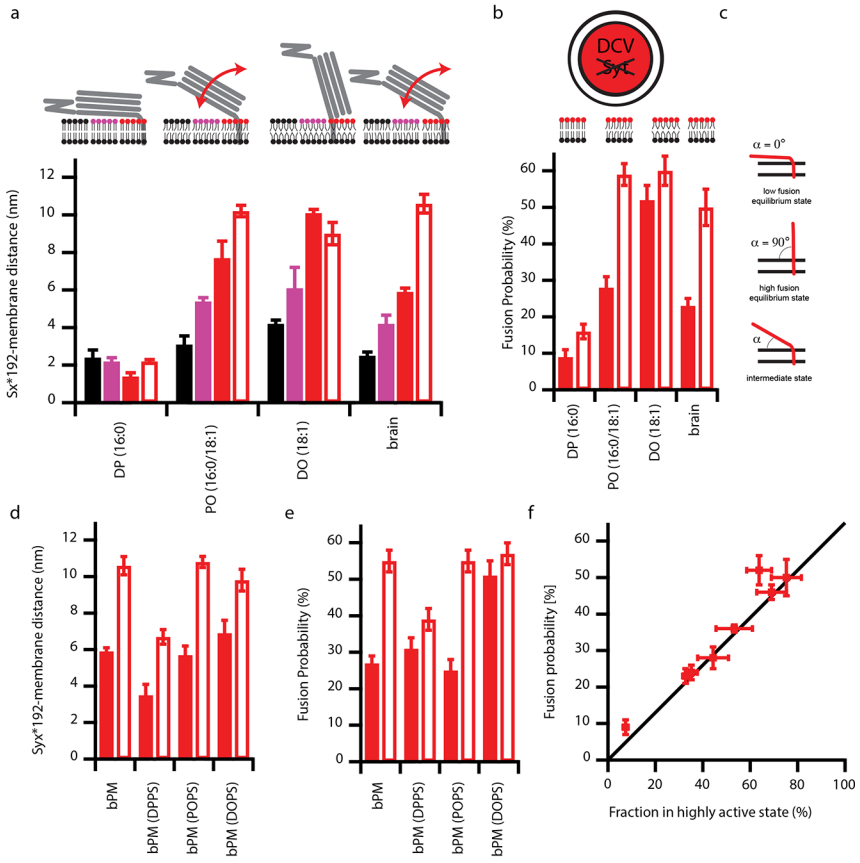

Fig. 3. Conformation of SNARE complex and DCV fusion depend on ratio between saturated and unsaturated fatty acids in target membrane.

a, Syx*192-membrane distances in different lipid headgroup and acyl-chain environments. The trans-mimicking SNARE complex was reconstituted into membranes containing either DP (all saturated), PO (mixed saturated/unsaturated), DO (all unsaturated), or bovine brain extract lipids. Three different headgroup compositions were tested: PC only (black), PC/PE (magenta) and plasma membrane mimicking (PM, red). Compositions are as indicated in the legend to Fig. 2b. Ca^{2+} and C2AB was added to the PM lipids (open bars). All membranes contained 20% cholesterol. b, Fusion probability of SytKD-DCVs with PM membranes of different acyl-chains before (solid bars) and after the addition of Ca^{2+}/C2AB. The cartoons on top encode the different headgroup compositions by color and schematically illustrate the acyl-chain order. c, Calculating the fraction of SNAREs in a highly active state by determining the angle between SNARE domain and membrane surface from the measured z-distances and the maximum extension of ~12 nm, that one would expect from the cis-SNARE crystal structure [32]. d, Syx*192-membrane distances in EDTA (solid bars) or Ca^{2+} and C2AB (open bars) in brain PM lipids with PS being either bPS, DPPS, POPS, or DOPS. e, Fusion probabilities of wild-type DCVs in EDTA (solid bars) or Ca^{2+} in brain PM lipids with PS being either bPS, DPPS, POPS, or DOPS. f, DCV fusion probabilities plotted versus the fraction of SNARE complexes in a highly active state. Data points were collected from single DCV fusion and sdFLIC experiments in lipid environments with PM headgroups in EDTA and from the C2AB titration in 100 μM Ca^{2+}. The solid line was calculated assuming

that 0% high fusion state results in no fusion and 100% high fusion state leads to the maximum observed fusion of ~65% under the conditions used in this work (Fig. 1e). All data represent means from at least 3 independent experiments (see Supplemental tables 1, 3 and 4 for details). Error bars represent s.e.m.

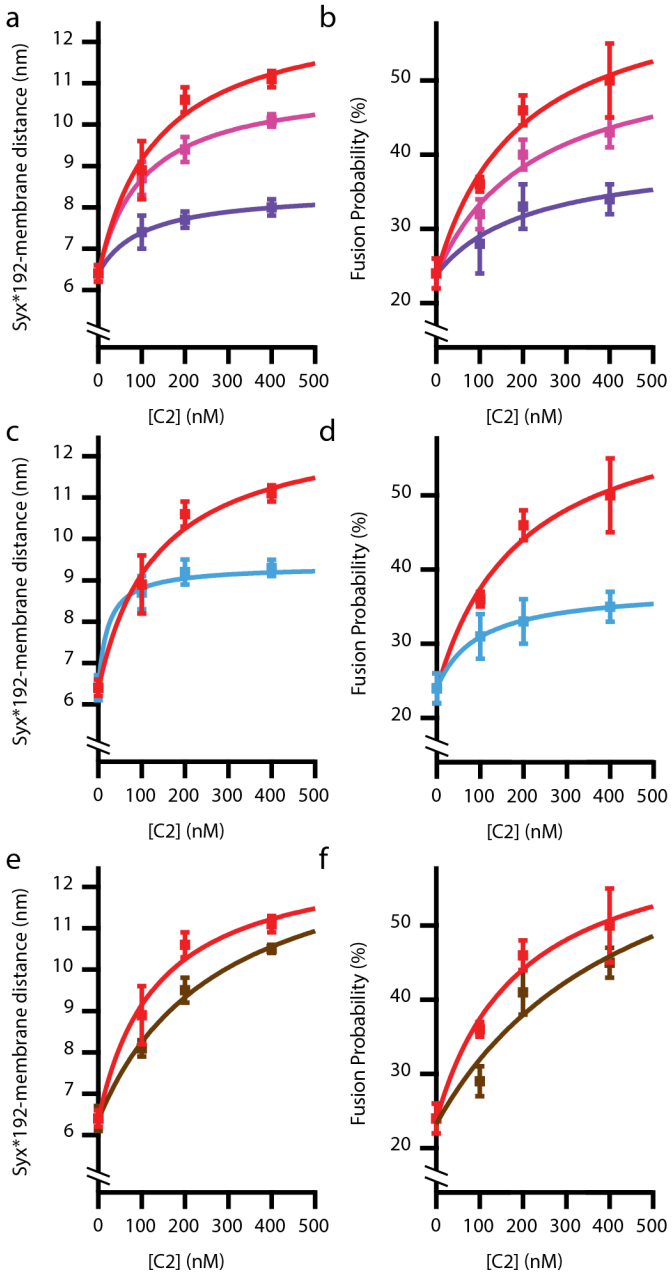

Fig. 4. Mutations in C2AB and SNAREs impair trans-cis conformational transition of SNARE complex and DCV fusion.

a, **b**, Syx*192-membrane distance changes and fusion probabilities of SytKD-DCVs observed in response to wild-type C2AB (red), C2B only (magenta), and C2A only (purple). **c**, **d**, Syx*192-membrane distance changes and fusion probabilities of SytKD-DCVs observed in response to wild-type C2AB (red) and C2AB-KAKA mutant where C2B function is ablated (cyan). **e**, **f**, Syx*192-membrane distance changes and fusion probabilities of SytKD-DCVs observed in response to wild-type C2AB (red) and C2AB-RQRQ mutant where proposed SNARE contact site is impaired (brown). All data represent

means from at least 3 independent experiments (see Supplemental tables 3 and 4 for details). Error bars represent s.e.m.

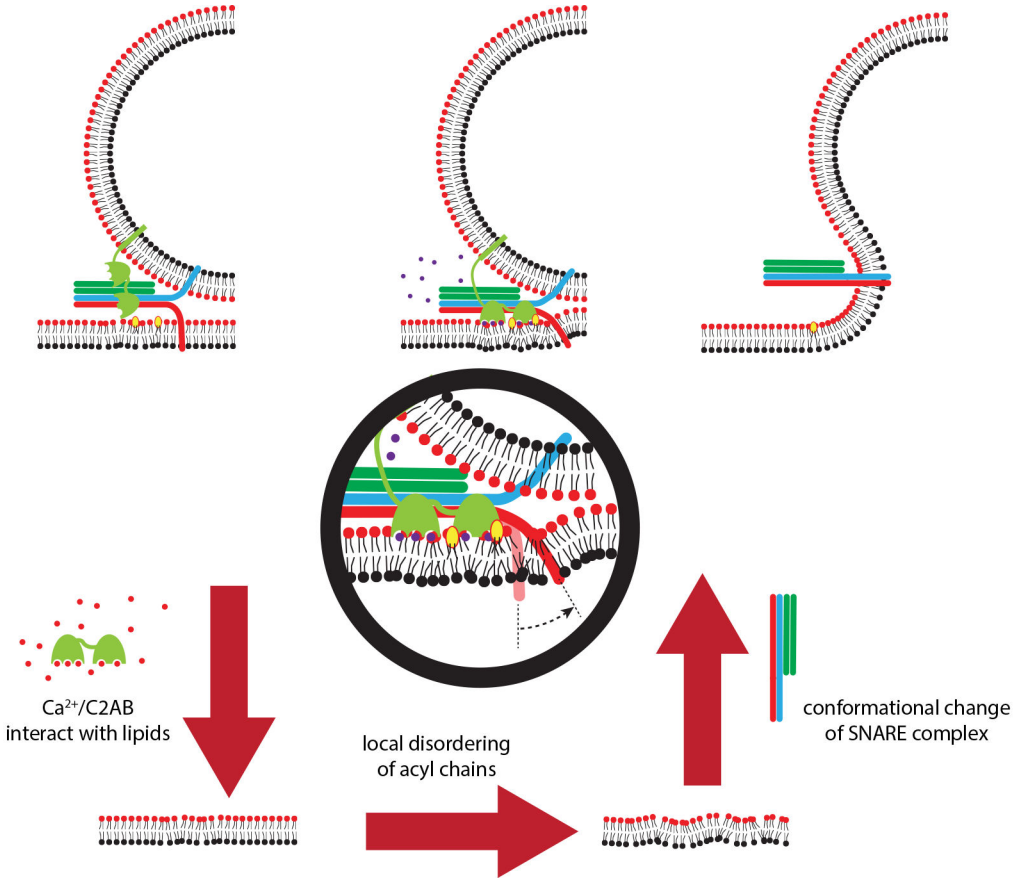

Fig. 5. Model for Ca^{2+}-triggered fusion mechanism.

When the vesicle is docked, in the absence of Ca^{2+}, the four-helical bundle of the SNARE complex is connected with the trans membrane anchors of syntaxin and synaptobrevin/VAMP via bent linkers in the juxta-membrane regions. In this trans-configuration, the C2B domain of synaptotagmin interacts with PI-4,5-P_2 in the target membrane. The C2 domains of multiple synaptotagmins might interact with each other and multiple SNARE bundles, in order to optimize the local alignment around the fusion site. After Ca^{2+} influx, the Ca^{2+} binding loops of the C2 domains insert into the membrane, causing local acyl-chain disorder and curvature in the bilayer near the fusion site. The disordering of the acyl chains induces a conformational change in the juxta-membrane linker region of syntaxin, inducing the trans-cis conformational transition of the SNARE complex that pulls the two membranes.